View metadata, citation and similar papers at core.ac.uk
brought to you by CORE
provided by Open Research Exeter

Development of a Strategy and Interpretation of the NIR Spectra for Application in Automated Sorting

Tinah PHIRI [a,*] , Hylke J. GLASS[a,] and Precious MWAMBA

Abstract

The potential of Near Infrared (NIR) spectroscopy for application in automated sorting was investigated on a sample of iron oxide copper-gold ore. The ore contains a substantial amount of carbonate material which results in excessive acid consumption in the leaching circuit during copper extraction, thereby increasing the processing cost. To separate this unwanted gangue material (carbonate) from the valuable metal (copper), a strategy for classification of ore according to copper and carbonate content was developed. The chemical and mineralogical composition of the ore was determined using XRF, respectively XRD. This data was correlated with NIR spectra measured on the surface of ore particles. NIR spectra showed distinct characteristic absorption features for carbonate rich particles that distinguish these from copper bearing particles, which are fairly featureless at longer NIR wavelengths (range 2000nm -2405nm). Combined interpretation of spectral features and chemical and mineralogical data indicates that NIR-based sorting has potential forthis type of ore.

1.0 Introduction

The mining industry is based on exploitation of non-renewable resources. There has been a significant decrease on the average grade in ore bodies over the years, creating more waste. This in turn has led to increased processing costs and decrease in productivity across the mining value chain(Carrasco et al., 2015).To make low feed grade ores economically viable and increase unit metal productivity, early elimination of course waste material before downstream concentration processes has been identified as an important operational advancement (Carrasco et al., 2014; Bowman and Bearman, 2014; Logan and Krishnan, 2012, Bearman, 2012).To achieve this, a new technique of sensor-based sorting is being investigated for pre-concentration of ore offering reduced processing costs, cut-off grade and environment impact for the mines (Salter and Wyatt, 1991).

The Near InfraRed (NIR) sensor offers rapid, inexpensive, non-destructive, non-invasive measurement of ore surfaces, with minimum sample preparation demands (Hunt, 1977).Interaction of near infrared electromagnetic waves with its constituents is considered to be robust for surface analysis (Hunt, 1977).It can help determine the mineralogy and provide information on the minor element chemistry of hard-to-discriminate carbonate minerals. As such, NIR provides a useful complement to existing mineralogical and petrographic methods for studying carbonates (Gaffey, 1986). In one step, NIR provides information which previously required combined application of two or more techniques. With a view to improving the sustainability of mineral processing operations through reduced energy and processing costs, this research seeks to develop a strategy to discriminate carbonate material (unwanted gangue) from the copper (product) through NIR spectral interpretation.

2.0 Material and methods

The ore material used in this experiment was from Northern Chile, America. With the carbonaceous material being the most problematic in the leaching circuit, copper was separated from carbonate. Proportions of the sample were made into 'high copper, low carbonate' and 'high carbonate, low copper' using the cluster algorithm.

2.1 NIR Spectroscopy

In light of the diverse nature of minerals, surface heterogeneity and complexity of the samples being investigated, ten transects were taken for each of the samples covering the entire surface on both sides. The belt was divided into an equal line labels spacing 10mm as shown in figure 3-1 below. Successive scans were made as the belt was being moved by hand to a predetermined marker point across the particle. A selected set of pure specimens taken from the Camborne School of mines learning lab for possible minerals present in the ore being tested were also scanned as spectra library and this was used as a guiding tool to examine spectral pattern, characteristic adsorption features and corresponding wavelengths for the samples. The spectral reflectance in near infrared sensors was measured when the material was illuminated by light and characteristic absorption features are then observed at specific wavelength for different minerals. Samples were analysed for presence of spectral features with appropriately characterised mineral samples.

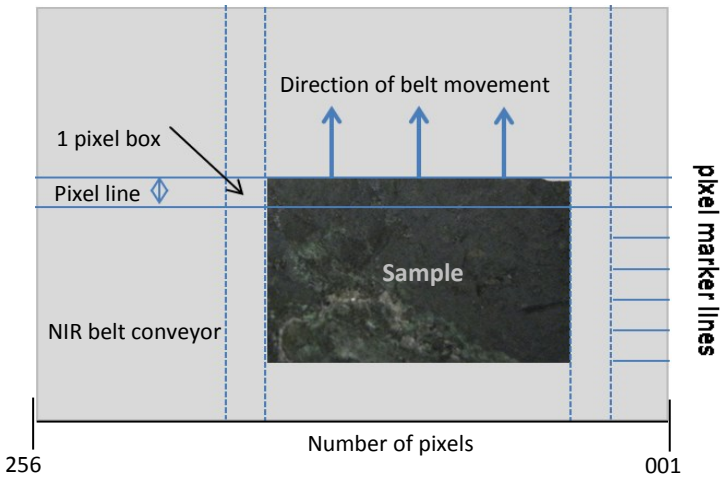

Figure 1: Schematic Representation of Sample and Pixel line location

2.1.1 Software and Pre- processing

The NIR data was collected using View2 software (Viewing programme 2). The data was produced in a Microsoft excel file, converted and formatted to comma separated value (csv). The raw images acquired by the camera needed to be pre-processed to correct the measurement deficiencies of the acquisition system and to reduce the amount of data for an efficient real-time classification. The process involved applying a correction factor to each wavelength in each pixel. There were two corrections: The first was a dark current correction (Dark Reading) and second was a detector calibration (White Reading) which was performed by measuring a white diffuse reflectance standard image. The resulting reflectance images could then have a resolution of 40 X 371 pixels corresponding to one spectrum (giving 371 vectors with 40 elements or less depending on the particle dimensions). The Visual Basic Application in excel was used to write and apply the algorithm.

2.1.2 Smoothing Techniques

The most important problem of using spectral data is signal noise levels. The physical disturbances such as the fluctuation of light illumination and atmospheric changes may also make the situation worse as the disturbances decrease the precision of spectral signals recorded by the sensor. In the field

of digital signal processing, the definition of a spectrum $s_o(\lambda)$ observed by a spectrometer is given by the sum of the true signal of the spectrum $s_t(\lambda)$ and the noise $n(\lambda)$ where λ indicates wavelength.

$$s_o(\lambda) = s_t(\lambda) + n(\lambda) \qquad \text{Egn.1}$$

Thus, the definition of spectral smoothing is the estimation of $s_t(\lambda)$ from the observed spectrum $s_o(\lambda)$. An estimate $\hat{s}_t(\lambda)$ can be calculated by the convolution of the observed spectrum $s_o(\lambda)$ with a weighting function (i.e. smoothing filter) $g(\lambda)$ chosen by the practitioner (Vaiphasa, 2006). The operator * denotes convolution integral,

$$s_t(\lambda) = s_o(\lambda) * g(\lambda) \qquad \text{Egn.2}$$

Spectral smoothing technique was used in this study remove the noise from the collected data. One of the samples was tested for noise levels at different windows. The figure below shows that unsmoothed pixels could have noise disturbances that may be mistaken for features and over smoothing could also completely smooth out the spectral features (e.g. 73window) which could lead to changes in the properties of the original data. In order to preserve the original properties of the spectral, smoothing filter window should then be careful considered. The moving average was used as a smoothing filter with a 7 filter window was used for this study

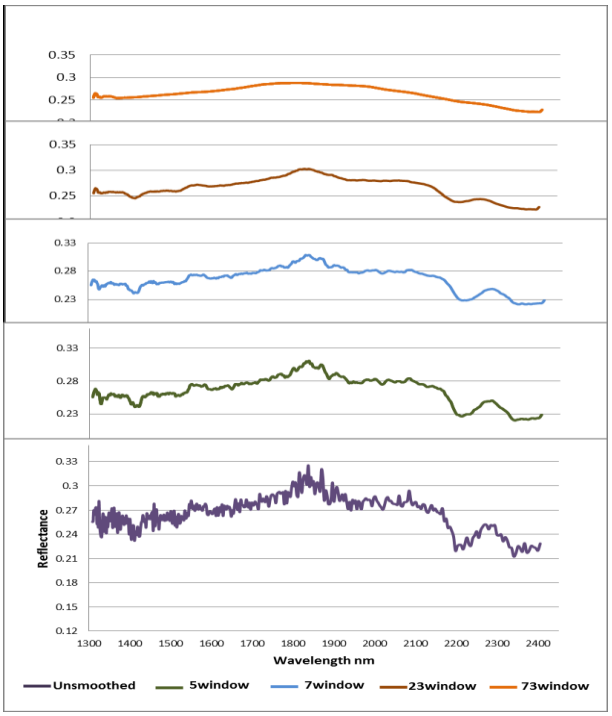

Figure 2: Spectral smoothing technique

2.2 *Chemical and mineralogical analysis*

The samples were prepared by standardised sample preparation techniques, fragmented using the laboratory jaw crusher and the disk grinder and then representative samples were taken from each of the resulting homogenised powders for analytical preparation. The boric jackets were prepared for XRF in order to analyse samples for chemical data and mineralogy of all samples was verified by XRD.

2.3 Material Classification

2.3.1 K-means Cluster Algorithm

The k-means cluster algorithm was used in this paper to computes the squared distances between the input data points and centroids, and then the input was assigned to the nearest centroid. The algorithm partitioned the input dataset into k clusters. Each cluster was represented by an adaptively-changing centroid, starting from some initial values named Seed-Points (Zalik, 2008). An algorithm for clustering N input data points into k disjoint subsets each containing in data points, 0 <ni<N, minimizes the following Mean-Square-Error (MSE) cost-function:

$$J_{\text{MSE}} = \sum_{i=1}^{k} \sum_{x_t \in C_i} \|x_t - c_i\|^2 \qquad \text{Egn.2- 13}$$

Where x_t is a vector representing the t-th data point in the cluster Ci and ci is the geometric centroid of the cluster C_i. This algorithm aims at minimizing an objective function, in this case a squared error-function, where $\|x_t\text{-}c_i\|^2$ is a chosen distance measurement between data point x_t and the cluster centre ci. The k-means algorithm assigns an input data point x_t into the ith cluster if the cluster membership function $I(x_t, i)$ is 1.

$$I(x_t, i) = \left\{ \begin{array}{ll} 1 & \text{if } i = \arg\min(\|x_t - c_j\|^2) \quad j = 1, \ldots, k \\ 0 & \text{otherwise} \end{array} \right\} \qquad \text{Egn.2- 14}$$

Here c_1, c_2, c_j…, ck are called cluster centres which are learned by the following steps illustrated by Zalik (2008): The four main steps included;

1. Initializing k cluster centres c1, c2..., ck using initial values called seed-points, through random sampling.
2. Calculating cluster membership function $I(x_t, i)$ by Equation (14) and decide the membership of each input data point in one of the k clusters whose cluster centre is closest to that point.
3. For all k cluster centres, ci was set to be the centre of mass of all points in cluster Ci.
4. For each input data point xt and all k clusters, steps 2 and 3 were repeated until all centres converge.

The first k-means cluster approach was a random selection of numbers which involved four modules and these includes;

- Data compilation- This compiled all the data samples into one sheet for training and number of pixels was identified for each particle. The k cluster centres were initialized by using random sampling. The centre of mass of all points in cluster was set for all k cluster centres.
- K-means Algorithms- computed the squared distances between the inputs data points and centroids, and assigned inputs to the nearest centroid and then the cluster membership function was calculated. To avoid initialising problem, the distance score was used as the measure of all data point to their cluster centroids.
- Tested compiled data- This was used to normalised the data
- Tested K-means- This was used to assign the numbers of pixels to the clusters.

The second k-means algorithm method was tried and this involved identifying the number of pixel that related to a particular particle. Cluster centres were initialised using a random number generator and members assigned to each cluster. The algorithm clustered each pixel individually. If there were no members in a cluster, the centre vector was set to null vector and if there were members in the cluster, then the centre is calculated. The current membership matrix was compared with the previous membership and if they converge the results were printed on the worksheet, otherwise another iteration was performed until convergence

2.3.2 *Cluster Validity*

Cluster validity as a measure of the quality of clustering, the David Bouldin (DB) Index was used. The clustering algorithm was run multiple times while varying the number of clusters in each run from minimum to maximum value. For each clustering obtained under this procedure the considered validation index was computed. Small values of DB correspond to clusters that are compact, and whose centres are far away from each other and the number of clusters that minimizes DB was taken as the optimal number of clusters, hence final results. Cluster validity was only applied to cluster algorithm1. The equation is given as below;

$$DB = \frac{1}{M}\sum_{i=1}^{m} \max_{j=1,\ldots,M;\, j\neq i}(d_{ij}), \text{ where } d_{ij} = \frac{\sigma_i + \sigma_j}{d(c_i, c_j)} \qquad \text{Egn.2- 15}$$

Where, M is the number of clusters, $d(c_i, c_j)$ is the distance of cluster centres c_i and c_j and σ_i is the average distance of all patterns in cluster i to their cluster centre c_i..

3.0 Results

3.1 Chemical Analysis on Selected Sample

The selection of the sample was done and classified according the cluster algorithms. Table 1 shows the XRF results based on the cluster classification. Hematite has been included due to its massive presence in this ore mainly on copper particles

Table 1: Mass fraction and (%) grade for selected samples

Sample name	Wt (g)	Cu (%)	CaO (%)	Fe_2O_3 (%)
PG01	766.40	0.38	0.27	20.47
PG02	500.30	0.00	21.57	5.5
PG03	352.50	0.14	21.70	4.86
PG04	583.10	0.00	23.52	5.46
PG05	711.40	0.15	8.80	8.21
PG06	488.90	0.00	22.24	9.37
PG07	687.90	4.01	7.77	16.71
PG08	670.70	0.58	5.11	5.2
PG09	790.70	3.26	20.78	20.14
PG10	707.30	0.16	18.08	5.84
PG11	790.10	0.00	11.94	3.41
PG12	268.30	0.15	23.24	5.7
PG13	300.00	0.19	16.26	4.04
PG14	419.10	0.13	0.27	14.64
PG15	1333.20	3.98	0.36	12.15
PG16	421.50	8.52	21.39	8.9
PG17	628.60	5.72	30.49	6
PG18	656.90	6.67	0.77	10.26
PG19	1120.90	2.49	0.33	15.25
PG20	888.10	0.25	0.13	6.97
PG21	377.60	0.20	1.34	10.45
PG22	535.30	0.00	3.77	15.43
PG23	619.70	1.02	0.16	6.09
PG24	572.10	0.18	0.19	6.62
PG25	874.60	1.06	0.00	58.76
PG26	467.00	1.55	0.15	31.49
PG27	798.50	4.73	0.18	35.2
PG28	1093.30	1.26	2.32	49.06
PG29	1358.60	1.03	0.00	49.38
PG30	1284.50	1.49	0.13	83.46
Total Feed	21067.10			
Feed grade	6.65%			

The samples were classified into product fraction (high copper, low carbonate and high copper, high carbonate) and Waste fraction (high carbonate, low copper and low copper, low carbonate). The cut-off grade for copper and carbonate was set at 1% and 5% respectively. The following classifications and sample number based on the cut-off grade could be considered economically viable;

Table 2: Material Classification

Category	Classification	Sample Number
Product	High Copper, low carbonate	PG18, PG19, PG23, PG25, PG26, PG27, PG28, PG29, PG30
	High Copper, high carbonate	PG07, PG09, PG15, PG16, PG17
Waste	High Carbonate, low copper	PG2, PG3, PG4, PG5, PG6, PG8, PG10, PG11, PG12, 13
	Low Carbonate, low copper	PG1, PG14, PG20, PG21, PG22, PG24

3.2 Mineralogical Analysis of the Ore

The mineralogy analysis identified seven most dominant crystalline mineral constituents present in the batch particles and these include: Calcite ($CaCO_3$), Quartz (SiO_2), Hematite (Fe_2O_3), Muscovite ($KAl_2(AlSi_3O_{10})(F,OH)_2$), Microcline ($KAlSi_3O_8$), Clinoclore ($(Mg,Fe^{2+})_5Al_2Si_3O_{10}(OH)_8$, and Cuprite ($Cu_2O$). The minor component includes; Malachite ($Cu_2CO_3(OH)_2$), Chrysocolla ($Cu_2H_2Si_2O_5(OH)_4$, Chlorite (ClO_2^-), Dolomite ($CaMg(CO_3)_2$), Dravite ($NaMg_3Al_6(BO_3)_3Si_6O_{18}(OH)_3F$), Sanidine ($KAlSi_3O_8$), Tenorite (CuO), Illite ($(K,H_3O)(Al,Mg,Fe)_2(Si,Al)4O10[(OH)_2,(H2O)]$, Magnitite ($Fe_3O_4$) and Apachite ($Cu_9Si_{10}O_{29}.11(H_2O)$).

3.3 NIR Spectral Interpretation

To select a region of the near infrared spectrum for analysis, library spectra for mineral present needed to be consulted and by examining spectra of pure specimens, characteristic peaks and the corresponding wavelength could be identified. Figure 3 below is a spectral of pure Malachite; the sample was taken from the Camborne School of Mines learning laboratory. Malachite has been selected because of its abundance as a copper mineral.

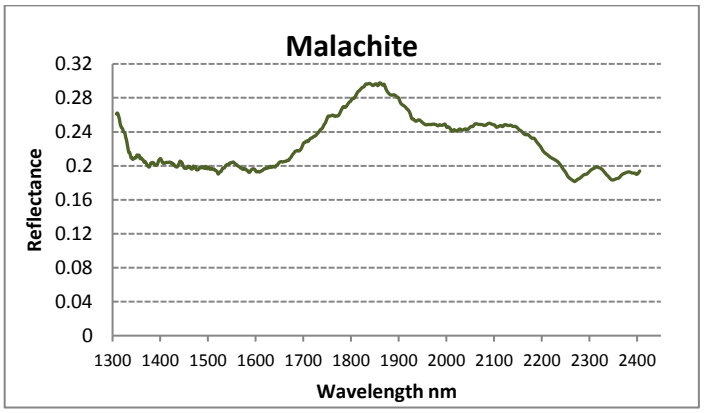

Figure 3: Spectral of Pure Malachite Specimen

Studying the spectra of malachite in figure 4-1 above by analogy with the spectrum of pure $CuCO_3$, the peak at 2270nm, 2350nm and 2370nm may be due to the CO_3 radical. Some contributions to the band at 2350nm and 2370nm may come from the hydroxyl present in this sample. The spectral range of (2000 -2405nm) was analysed for these samples because it is considered to offer significant information about minerals.

3.3.1 NIR Spectral Interpretation: High Copper Samples

The spectral interpretation and Photomicrographs analysis for the high copper samples combined with the indicative composition of XRF and XRD results for individual particles. The photomicrographs have been presented with the scale taken on the microscope for all the particles to show that only a small area was focused to be representative of the entire particle and this area does not represent the entire spectra seen in the samples but only a small section. This could be estimated for a single pixel dimension covering about 14mm in size.

Table 2: PG9 Indicative Composition

Analysis	**Indicative Sample Composition- PG9**					
XRF	Cu	CaO	Fe_2O_3	Al_2O_3	SiO_2	LOI%
(wt%)	3.26	20.78	20.14	7.86	25.79	16.96
XRD	Quart, Microcline, Malachite, Clinochlore, Calcite, Cuprite					

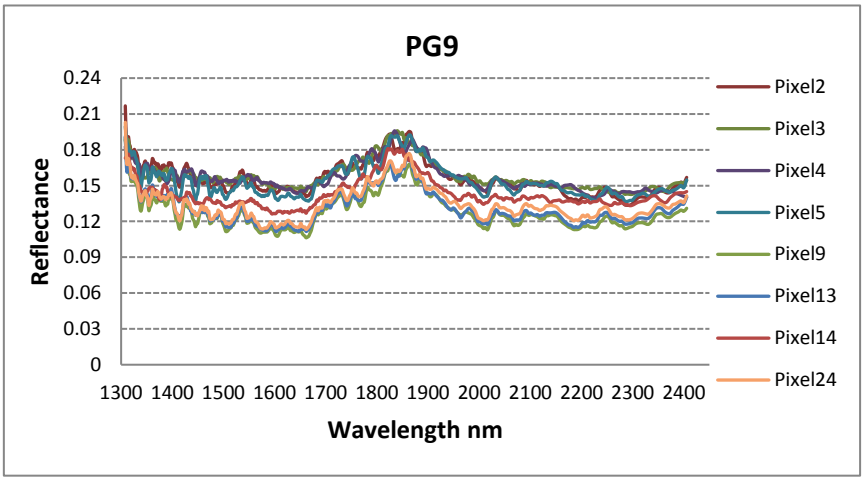

Figure 4: Plot of NIR reflectance against wavelength for Sample PG9

Figure 4 present a copper-carbonate-iron rich sample. The limitation in the relative reflectance and the lack of distinct features is apparent in this sample. Iron and calcite indicates about the same content and dominating the entire matrix. This sample only has a weak features appearing at about 2000 to 2050nm which may be due to low frequency lattice modes of the OH stretching fundamental. And a weak carbonate feature at about 2375nm which may be due to CO_3^{2-} anion present in malachite. This is one of the samples indicated with high copper, high carbonate presented XRF results classified as product. The cluster algorithms does indicate that the carbonate content in this sample is only about 10% compared to the copper content which is also supported with spectral interpretation.

Table 3: PG15 Indicative Composition

Analysis	**Indicative Sample Composition- PG15**					
XRF	Cu	CaO	Fe_2O_3	Al_2O_3	SiO_2	LOI%
(wt%)	3.98	0.36	12.15	14.86	57.91	4.56
XRD	Quart, Muscovite, Hematite, Cuprite					

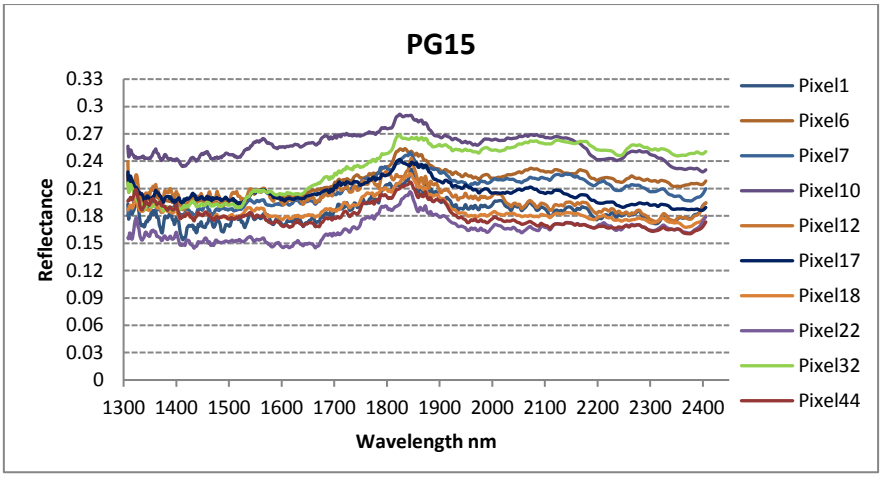

Figure 5: Plot of NIR reflectance against wavelength for Sample PG15

Samples PG15 present a copper rich, low carbonate particle with significant iron staining due to hydrothermal alterations. The copper is present in the sample in cuprite form. The sample is equally featureless with only few weaker bands at about 2200nmdue to Al-OH present in muscovite or this may also be due to H-O vibrations, and a high correlation to this spectral indicate the presence of hematite due to drop in reflectance and 2290nm may arise from the Fe-OH.

Table 4: PG18 Indicative Composition

Analysis	**Indicative Sample Composition- PG18**					
XRF	Cu	CaO	Fe_2O_3	Al_2O_3	SiO_2	LOI%
(wt%)	6.67	0.77	10.26	8.72	58.78	6.47
XRD	Quart, Malachite, Tenorite, Clinoclore					

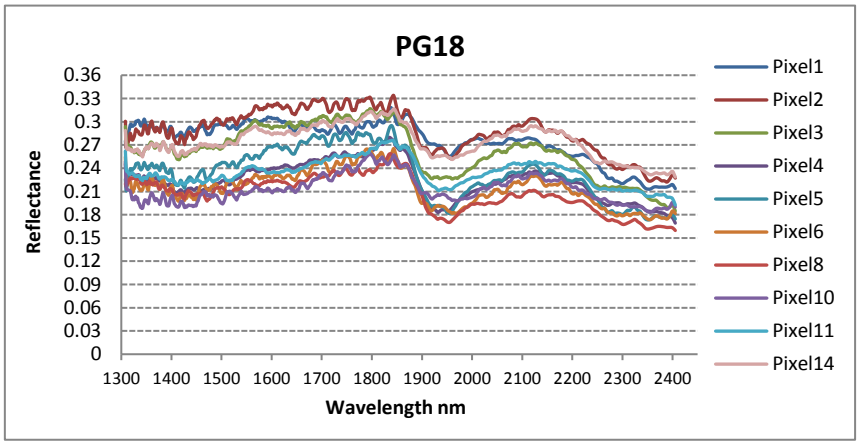

Figure 6: Plot of NIR reflectance against wavelength for Sample PG18

Sample PG18 in the figure above indicates a high copper, low carbonate particle on a quartz matrix. This is one of the few high copper samples with indicative composition of low iron as most of the copper particles have been shown to occur in association with the iron oxides. The presence of a carbonate features at wavelength 2350nm and 2375nm is indicative of the malachite present in the sample. The deep broad peak at 1900-1950nm is due to combinations of the H-O-H band with the OH stretches due to the water molecule. This is an example of high copper samples, which cannot be understood by spectra interpretation alone because of the band broadening, leading to complex spectra and making it difficult to assign specific features to specific chemical components without any analysis technique.

Table 5: PG19 Indicative Composition

Analysis	Indicative Sample Composition- PG19					
XRF (wt%)	Cu	CaO	Fe_2O_3	Al_2O_3	SiO_2	LOI%
	2.49	0.33	15.25	15.78	45.88	5.285
XRD	Quartz, Hematite, Microcline, Clinochlore, Cuprite					

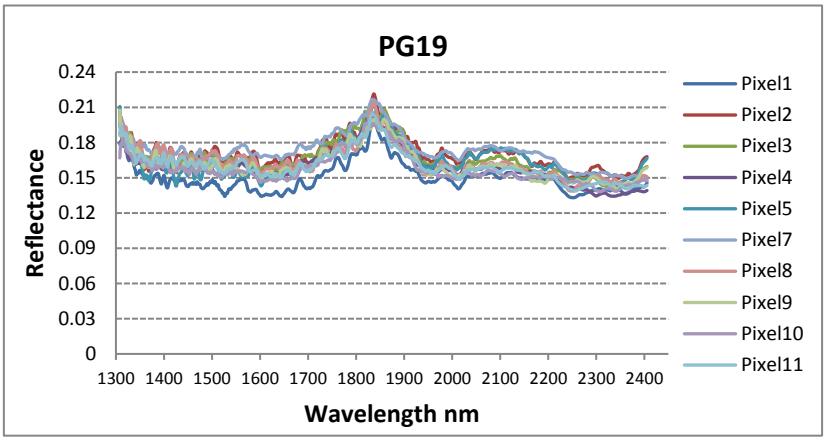

Figure 7: Plot of NIR reflectance against wavelength for Sample PG19

The notable spectral features correlate to the observable surface mineralogy shows fine grain copper dissemination with iron crystals and silicates. Figure 7 presents a copper rich particle indicated by the presence of cuprite (green colouring) in this sample and similarly no spectral pattern is observed in this sample due to quartz matrix and the presence of hematite dominating the spectrum.

Table 6: PG30 Indicative Composition

Analysis	Indicative Sample Composition- PG30					
XRF (wt.%)	Cu	CaO	Fe_2O_3	Al_2O_3	SiO_2	LOI%
	1.49	0.13	83.46	3.08	9.21	3.245
XRD	Quartz, Hematite, Microcline, Clinochlore					

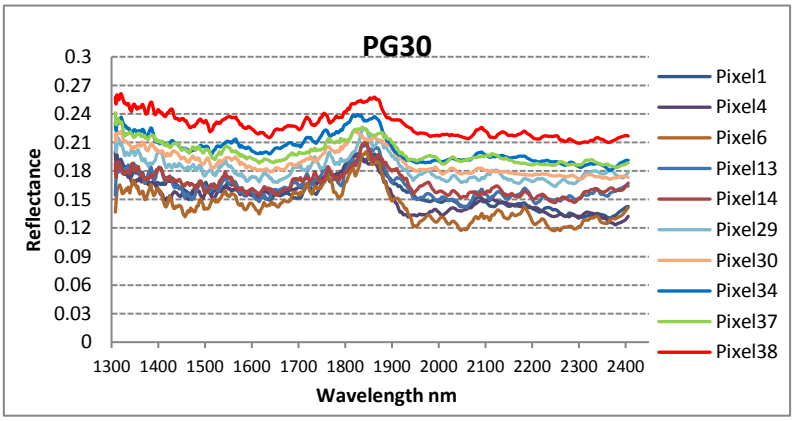

Figure 8: Plot of NIR reflectance against wavelength for Sample PG30

Sample PG30 is a relative high copper-rich particle and featureless with its iron content increasing with decreasing reflectance. It can also be observed from this sample that it has the amount of iron which is way too high with for example 83.46%Fe and clearly indicating low reflectance ranging from 0.1 -0.27.

4.4 Results: High Carbonate Samples

4.4.1 Introduction

The most common of the carbonate minerals is Calcite. Figure 9 below shows the pure calcite sample taken from the Camborne School of Mines laboratory. It was scanned in order to be used as spectral library. Pure calcite only exhibits spectral bands at a longer wavelength. These bands can be seen at 1800 to 2400nm in the figure below;

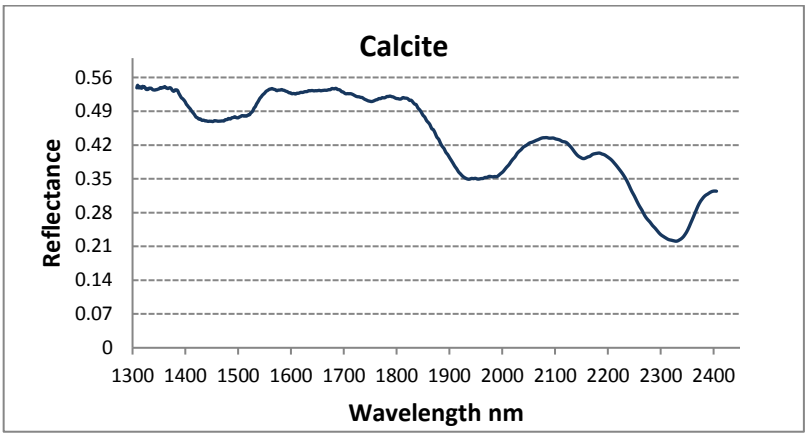

Figure 9: Spectral Library of Pure Calcite

Notable features in the figure 9 above are the ones indicated at 1600nm, 1730nm, 1800nm, 1900nm, 2000nm, 2150nm and intense band between 2300- 2350nm. The deep absorption observed between 1400nm -1500nm is the overtones of the OH stretches and combinations of the H-O-H band with the OH stretches are found at about 1900nm due to water molecules. It should be noted that the spectral appearance of this calcite is different from the one indicated in figure 2-3 which could be due to difference in the purity of the sample and internal calibration of the equipment. Analysis of the carbonate spectral with their indicative composition and photomicrographs could now be presented after though understand of spectral library of predominant mineral in this section.

4.4.2 Spectral Interpretation: Carbonates

The spectral interpretation analysis for the high carbonate samples combined with the indicative composition of XRF and XRD results for individual particles.

Table 7: PG2 Indicative Composition

Analysis	**Indicative Sample Composition- PG2**					
XRF	Cu	CaO	Fe_2O_3	Al_2O_3	SiO_2	LOI%
(wt%)	pmm	21.57	5.5	13.43	37.14	16.8
XRD	Quartz, Calcite, Clinochlore, Muscovite					

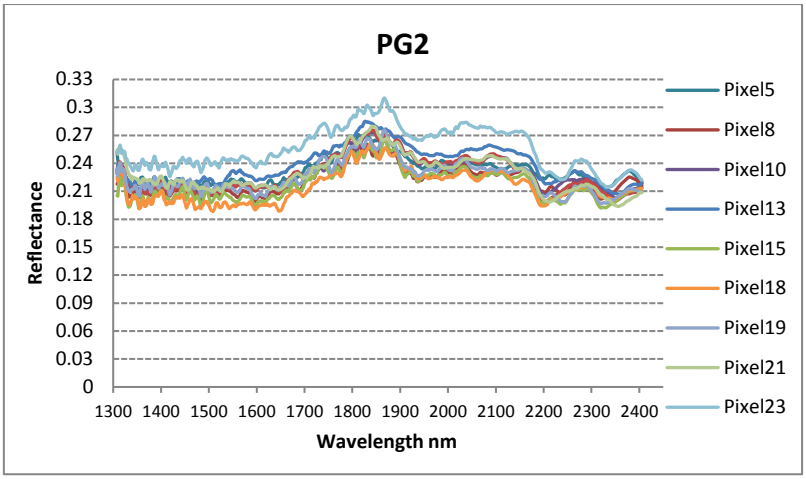

Figure 10: Plot of NIR reflectance against wavelength for Sample PG2

Sample PG2 in figure 10 is atypical of a carbonate-rich particle. It displays peaks at 2200nm, 2300nm and 2375nm. The peak at 2200nm indicates the presence of Al-OH which is found in Muscovite confirmed herein by XRD results meanwhile the peak observed at 2300nm is due to the presence of Mg-OH or conversely carbonates which may occur between 2300nm and 2375nm.

Table 8: PG4 Indicative Composition

Analysis	**Indicative Sample Composition- PG4**					
XRF	Cu	CaO	Fe_2O_3	Al_2O_3	SiO_2	LOI%
(wt%)	ppm	23.52	5.46	11.39	37.99	17.6
XRD	Quartz, Calcite, Clinochlore, Muscovite					

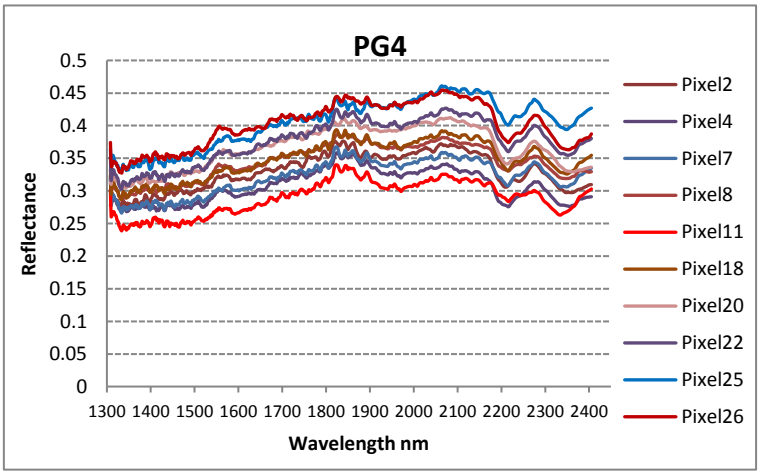

Figure 11: Plot of NIR reflectance against wavelength for Sample PG4

Sample PG4 in figure 11 has a more intense peak at about 2200nm indicating the presence of Al-OH due to the Muscovite present in this sample. The other features observed are at about 2245nm, and weak band at about 2350nm. The weak peak at 2245nm could due to O-H affected by either silicon or iron in clinoclore. The band at 2350nm is likely to be O-H stretch shifted due to interaction with the magnesium in clinoclore or due to presence of calcite.

Table 9: PG5Indicative Composition

Analysis	Indicative Sample Composition- PG5					
XRF (wt%)	Cu	CaO	Fe_2O_3	Al_2O_3	SiO_2	LOI%
	0.15	8.8	8.21	17.66	48.99	8.62
XRD	Quartz, Calcite, Microcline, Clinochlore, Muscovite, Illite, Hematite, Hydroxylapatite					

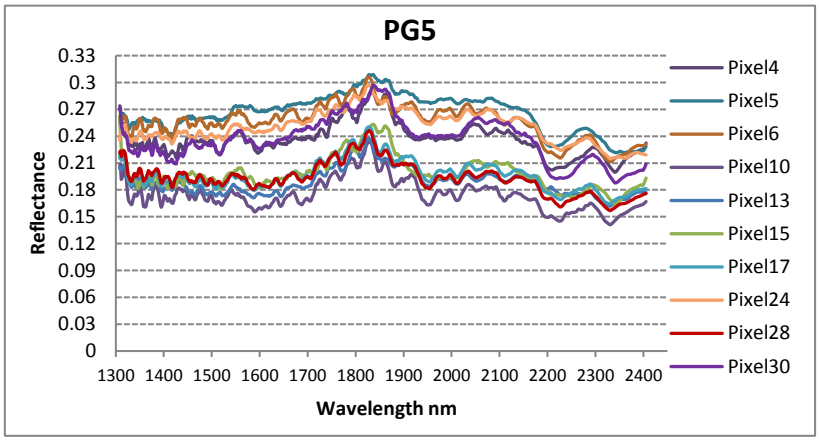

Figure 12: Plot of NIR reflectance against wavelength for Sample PG5

Sample PG5 exhibited peaks in the vicinity of 2200nm, and 2330nm. The peak at about 2200nm is due to Al-OH stretch present in muscovite, and the band at 2330nm may be due to the Mg-OH stretch present in clinoclore/illite. The cross correlation with XRD results does indicate the presence of these minerals.

Table 10: PG6 Indicative Composition

Analysis	Indicative Sample Composition- PG6					
XRF (wt%)	Cu	CaO	Fe_2O_3	Al_2O_3	SiO_2	LOI%
	ppm	22.24	9.37	13.4	36.63	16.6
XRD	Calcite, Quartz, Muscovite, Illite, Hematite, Dravite					

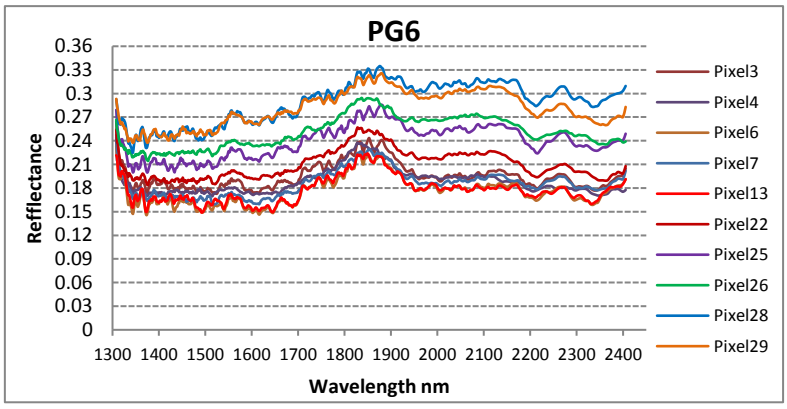

Figure 13: Plot of NIR reflectance against wavelength for Sample PG6

Sample PG6 is equally a carbonate-rich particle with its spectral features appearing at 2200nm, and 2330nm. The peak present at 2200nm is due to the Al-OH in Muscovite and the band displayed at 2330nm is essentially the same as one in PG5 resulting from the O-H stretch shifted due to interaction with the magnesium in clinoclore present in this sample which could also indicate the presence of calcite.

4.0 Discussion

The variety of absorption processes and their wavelength dependence was used to derive information about the chemistry of a mineral from its reflected light. The absorptions observed in the near infrared spectrum are due to vibrational processes (overtones and combination tones of the fundamental modes occurring in the near infrared) of anion groups and molecules such as OH^-, CO_3^{2-} and H_2O (Hunt and Salisbury, 1971). The atomic groups form independent oscillatory units such as Al-OH, Mg-OH and CO_3 observe on different bands position. Most of the sample have shown the broad feature around 1800nm - 1900nm which is of little significance as this study was mainly focused on a wavelength range of 2000 – 2405nm where there is significant information and that is why nothing much has been elucidated on this particular area. Clark (1995) noted that most low grade rock type exhibit a peak at 2200nm to 2210nm this has also been observed in this study due to the massive presence of muscovite giving the Al-OH stretching mode. The region between 2200–2500 nm of the spectral bands are ascribed to the OH stretch fundamental in combination with either the fundamental of SiO_2 stretch or a metal–OH bend (Hunt, 1977).

It has been indicated that most copper minerals have no features in the Near Infrared region with only features being observe when a copper particle has a matrix dominated by Malachite crystals. The relative reflectance intensities of the copper samples have also been observed to be generally low for all the samples ranging from about 0.09 -0.35. This could have been due to the iron being mostly associated with the copper particles. The presence of iron in other minerals could also lead to loss in relative reflectance depending on the type of minerals present in sample and the sample brightness. Calcite has been shown to have a very high reflectance (0.21-0.55) because of its brightness. This could be due to the presence of hematite dominating the spectrum. Bishop et al (1996) demonstrated that the presence of the hematite suppresses certain peaks that appear in the near infrared spectrum depending on the iron content.

Surface heterogeneity and complexity may also lead to inaccuracy. On the other hand, the mineral surface could be homogenous but contains an inclusion, and if the transect is taken on that particular area then the analysis of transect would be incorrect. The environmental parameters such as temperature, pressure, and orientation can also affect the appearance of the spectra (Clark, 1995). Another factor that can cause spectral of mineral mixtures difficult to interpret is that the mineral dominacnce in the particle does not always mean the same mineral would dominate the spectra (Bishop and Dummel, 1996)

5.0 Conclusions

The k-means cluster algorithms used in this study successful classified the material using two clusters into high copper, low carbonate and low copper, high carbonate. The combination of mineralogical and chemical analysis with the NIR spectra qualitatively analysed the material by relating them to the different mineral types present in the ore.

The strategy identified distinct characteristic absorption features depending on the reflectance on the mineral particles at a specific wavelength. This indicates that through interpretation of the adsorption features, the near infrared has potential in discriminating the carbonate particles (unwanted gangue) from the copper bearing particles (Product) which are fairly featureless at longer wavelength (range 2000nm -2405nm). This then implies that the mining industry can reduce processing costs on high energy intensive comminution, water and concentration through early rejection of unwanted gangue material. This could lead to an economic gain through reduced processing cost and increased productivity per unit metal produced.

Acknowledgements

The authors wish to thank the Zambia government and the Copperbelt University management for the financial support towards this research and Camborne School of Mines staff for the expertise and guidance.

6.0 References

Arvidson, B. 2002.Photometric ore sorting.*Mineral Processing Plant design, Practical and Control*, edited by A.L Muller, D.N. Halbe and D.J. Barratt (SME).

Bishop and Dummel. 1996. The influence of fine grained Hematitepowder on the Spectral properties of Mass soil Analogs. *VIS-NIR Bi-Directional Reflectance Spectroscopy of mixtures, 27. 119-120.*

Bowman, D.J., and Bearman, R.A., 2014. Coarse waste rejection through size based separation. Minerals Eng. 62, 102–110.

Carrasco, C., Keeney, L., Walters, S., 2014. Development of a novel methodology to characterise preferential grade by size deportment and its operational significance. Miner Eng. (2015)

Clark, R. 1995.Reflectance Spectral.*United States Geological Survey*. 178 -188.

Gaffey, S. J. 1986. Spectral Reflectance of Carbonate Minerals in the Visible and Near Infrared (0.35-2.55 microns): Calcite, Aragonite, and Dolomite. *American Mineralogist, Volume 71*, 151-162.

Gaydon, J. H., H.J Glass and R.D Pascoe.2009. Method for Near Infrared Sensor Based Sorting of Copper ore. Journal of near infrared spectroscopy, 177-194.

Hunt, G.R. 1977. Spectral Signatures of Particulate Minerals in the Visible and Near Infrared*Geophysics, Vol. 42*, 501-511, 10 FIGS.

Hunt, G.R. 1979. Near-infrared (1.3-2.4 pm) Spectra of alteration Minerals-Potential for use in Remote Sensing: *Geophysics, Vol. 44*, 1974-1986, 13 FIGS.

Hunt, G.R., and J.W. Salisbury. 1979. Visible and Near Infrared Spectra of Minerals and Rocks: I Silicates. *Modern Geology 2*, 283-300.

Hunt, G.R., and J.W. Salisbury. 1971. Visible and Near Infrared Spectra of Minerals and Rocks: II. Carbonates;*Modern Geology 2*, 23-30.

Hunt, G.R., and J.W. Salisbury., C.J. Lenhoff,. 1971. Visisble and Near Infrared Spectra of Minerals and Rocks: III. Oxides and Hydroxides.*Modern Geology 2*, 195-205.

Iyakwari, S., Glass, H.J., 2014. Influence of mineral particle size and choice of suitable parameters for ore sorting using near infrared sensors. Miner. Eng. 69,102–106.

Iyakwari, S., Glass, H.J., 2015. Mineral preconcentration using near infrared sensor based sorting. Physicochem. Probl. Miner. Process. 51 (2), 661–674.

Pascoe.R.D., O.B. Udoudo, H.J. Glass. 2010. Efficiency of Automated Sorter Performance Based on Particle Proximity Information. *Estimating sulphide ore grade in broken rock using visible/infrared hyperspectral reflectance spectra*.

Pasquini, C., 2003. Near Infrared Spectroscopy: Fundamentals, Practical Aspects and Analytical Applications.Instituto de Química, UniversidadeEstadual de Campinas, Brazil. Vol. 14, No. 2, 198-219.

Salter, J.D., and N.P.G. Wyatt. 1991. Sorting in the Minerals Industry: Past, Present and Future, *Mineral Engineering 4,* 779–796, Pergamon Press, Great Britain

Vaiphasa, C. 2006. Consideration of smoothing techniques for hyperspectral remote sensing.*Photogrammetry & Remote Sensing 60*, 91–99.

Wills, B.A., and J.T. Napier- Mann.2006 .Mineral Processing Technology – An Introduction to the Practical Aspects of Ore Treatment and Mineral Recovery.*Butterworth-Heinemann. Seventh Edition,* 373-375

Zalik, K.R., 2008. An Efficient K-means Clustering Algorithm. *Pattern Recognition Letters 29,* 1385–1391.